Langevin-Poisson-EQT: A dipolar solvent based quasi-continuum approach for electric double layers

S. Y. Mashayak and N. R. Aluru

Citation: J. Chem. Phys. **146**, 044108 (2017); doi: 10.1063/1.4973934
View online: http://dx.doi.org/10.1063/1.4973934
View Table of Contents: http://aip.scitation.org/toc/jcp/146/4
Published by the American Institute of Physics

Langevin-Poisson-EQT: A dipolar solvent based quasi-continuum approach for electric double layers

S. Y. Mashayak and N. R. Aluru[a)]
Department of Mechanical Science and Engineering, Beckman Institute for Advanced Science and Technology, University of Illinois at Urbana-Champaign, Urbana, Illinois 61801, USA

(Received 29 September 2016; accepted 29 December 2016; published online 25 January 2017)

Water is a highly polar solvent. As a result, electrostatic interactions of interfacial water molecules play a dominant role in determining the distribution of ions in electric double layers (EDLs). Near a surface, an inhomogeneous and anisotropic arrangement of water molecules gives rise to pronounced variations in the electrostatic and hydration energies of ions. Therefore, a detailed description of the structural and dielectric properties of water is important to study EDLs. However, most theoretical models ignore the molecular effects of water and treat water as a background continuum with a uniform dielectric permittivity. Explicit consideration of water polarization and hydration of ions is both theoretically and numerically challenging. In this work, we present an empirical potential-based quasi-continuum theory (EQT) for EDL, which incorporates the polarization and hydration effects of water explicitly. In EQT, water molecules are modeled as Langevin point dipoles and a point dipole based coarse-grained model for water is developed systematically. The space dependence of the dielectric permittivity of water is included in the Poisson equation to compute the electrostatic potential. In addition, to reproduce hydration of ions, ion-water coarse-grained potentials are developed. We demonstrate the EQT framework for EDL by simulating NaCl aqueous electrolyte confined inside slit-like capacitor channels at various ion concentrations and surface charge densities. We show that the ion and water density predictions from EQT agree well with the reference molecular dynamics simulations. *Published by AIP Publishing.* [http://dx.doi.org/10.1063/1.4973934]

I. INTRODUCTION

When an electrolyte fluid, which is usually an aqueous solution of ions, interacts with a charged surface, the surface electric field attracts counter ions to form a layer of counter ions near the surface, which is called the "electric double layer" (EDL).[1] EDL is fundamental to many technological applications, such as energy storage devices,[2,3] water desalination,[4,5] and biological systems.[6] Structural, electrochemical, and transport properties, e.g., density, capacitance, charge transfer, reaction rates, and viscosity, play an important role in the design and application of the electrolyte systems. These properties are governed by molecular physics of EDL at the length scales ranging from a few Angstroms to several nanometers. Therefore, to design electrochemical systems, it is critical to understand molecular origins of the properties of EDL.

Theory and computational tools are essential to interpret and analyze experimental data, and to obtain molecular level insights, which may not be accessible via experiments. Molecular simulation tools, such as molecular dynamics (MD) and Monte Carlo (MC) simulations, allow a detailed atomic-level study of EDLs.[7,8] However, it is computationally expensive to perform atomistic simulations of electrolyte systems, especially for low ionic concentrations which require enormous number of solvent molecules. For example, simulations of 10 mM ion concentration require thousands of water molecules per ion, and due to low ion counts, long simulations are required to achieve reliable statistics. Therefore, we need theoretical models which are not only simple and computationally faster than molecular simulations but also physically accurate.

The Gouy-Chapman (GC) theory based on the Poisson-Boltzmann (PB) equation is the most basic and popular theory to study EDL.[9] It models ions as point charges and incorporates only the electrostatic interactions among them; furthermore, it treats water implicitly as a background medium with a uniform dielectric permittivity. However, it ignores many important molecular aspects of the fluid, such as finite size of the ions, statistical correlations, the van der Waals (vdW) interactions, molecular nature of water, and variations in the dielectric permittivity. Therefore, the accuracy of the Gouy-Chapman theory is limited.

To address the limitations of the GC theory, various advanced theories have been developed, such as the modified PB theory,[10] integral equation theory,[11] and classical density functional theory (cDFT).[12–17] These theories, in addition to the electrostatic interactions, mainly account for the finite size effects of ions and van der Waals interactions among them. However, they usually ignore molecular details of water and variations in the dielectric permittivity. For example, in the most common cDFT approach, which is also known as a primitive model (PM), ions are modeled as charged hard spheres, water is treated as a background continuum with a uniform dielectric permittivity, and then the ion density profiles and EDL properties are obtained by minimizing a free energy

a)Electronic mail: aluru@illinois.edu

functional.[18] In the PM, if all the ions are assumed to have the same hard sphere diameter then it is called a restricted PM (RPM).[19]

The implicit solvent-based methods ignore important molecular details of water and, hence, they fail to predict several key experimental[20] and atomistic simulation results.[7,21] Near a surface, water molecules are packed in distinct density layers, and they exhibit anisotropy in their orientations.[22,23] Such inhomogeneous and anisotropic arrangement of the interfacial water molecules gives rise to pronounced oscillations in the polarization, dielectric permittivity, electric field, and hydration interactions near the surface.[24,25] Consequently, the interfacial water has a dominant effect on the electrostatic and hydration energies of ions, which in turn affect the spatial arrangements of ions and electrostatic potential and capacitance of EDL. Therefore, the representation of water as a homogeneous dielectric medium is inaccurate. To accurately predict the properties of EDL, it is necessary to consider molecular details of water explicitly.

There are some approaches which try to incorporate molecular details of water explicitly. The simplest approach is to model water molecules as hard spheres with uniform dielectric permittivity. A hard sphere water model has been used in various cDFT-based studies of EDL, which are also known as three component model (3CM) or molecular solvent model (MSM).[26,27] Lee *et al.*[14] have further incorporated the Lennard-Jones (LJ) interactions among ions, water, and wall particles in the 3CM cDFT. However, the hard sphere model is a very crude approximation for a water molecule, and it ignores water-water electrostatic interactions and variations in the orientation and dielectric permittivity of water. To include water orientation and polarization effects, dipolar solvent-based approaches have been proposed, such as the Langevin dipole model,[28–30] dipolar hard sphere model based on mean spherical approximation (MSA),[31] and dimer solvent-based cDFT.[32] Accuracy of these dipolar solvent-based approaches is limited. For example, dipolar hard sphere MSA is a linear response theory and is limited to small surface charge densities.[33] Moreover, a detailed comparison of the dipolar solvent-based theories with higher fidelity MD simulations has not been performed.

In this work, we present an empirical potential-based quasi-continuum theory (EQT) for EDL, which can accurately incorporate the molecular effects of water on the arrangement of ions in EDL. In earlier work, EQT has been shown to accurately predict the properties of confined fluids, such as simple LJ fluids,[34–37] CO_2,[38] and water.[39,40] Here, we extend the EQT framework to include the effects of water dipole orientation, polarization, and dielectric permittivity variation near a charged surface. To explicitly incorporate water polarization effects, we systematically develop a point dipole based coarse-grained (CG) model of water. We also develop coarse-grained ion-water potentials to accurately capture ion hydration effects. We show that EQT with point dipole water model and ion-water coarse-grained potentials can accurately predict the density profiles of water and ions near a charged surface.

The remainder of the paper is organized as follows. In Sec. II, we describe the EQT framework for EDL. In Sec. III, we provide the details of systematic coarse-graining to develop a point dipole water model and ion-water coarse-grained potentials. In Sec. IV, we describe the numerical details of EQT and the reference MD simulations. In Sec. V A, we provide the analysis of the point dipole approach to predict the electrostatic potential profile in EDL. In Sec. V B, we demonstrate the EQT approach by simulating the NaCl aqueous electrolyte confined inside slit-like capacitor channels at various ion concentrations and surface charge densities. Finally, we draw conclusions in Sec. VI.

II. EQT FOR EDL

Consider a mixture of cations (+), anions (−), and water (w) molecules confined in a charged slit channel. At equilibrium, the distribution of the fluid molecules is given by the 1-D Nernst-Planck (NP) equation

$$\frac{d}{dz}\left(\frac{d\rho_i}{dz} + \frac{\rho_i}{k_B T}\frac{dU_i}{dz}\right) = 0, \tag{1}$$

with boundary conditions

$$\rho_i(0) = 0, \tag{2a}$$

$$\rho_i(L) = 0, \tag{2b}$$

$$\frac{1}{L}\int_0^L \rho_i(z)\,dz = \rho_{i,\text{avg}}, \tag{2c}$$

where ρ_i and U_i are the density and total potential of the molecule i (= +, −, w), respectively, T is the fluid temperature, k_B is the Boltzmann constant, L is the channel width, $\rho_{i,\text{avg}}$ is the average density of the molecule i inside the channel, and z-axis is normal to the wall. The solution of Eqs. (1) and (2) is equivalent to the solution of the Boltzmann distribution equation,

$$\rho_i(z) = \rho_{i,\text{ref}} \exp\left(-\frac{U_i(z) - U_{i,\text{ref}}}{k_B T}\right), \tag{3}$$

where $\rho_{i,\text{ref}}$ and $U_{i,\text{ref}}$ are the reference density and potential of the molecule i, respectively. For the electrolyte system, the total potential energy can be split into the electrostatics, $U_{i,\text{elec}}$, and van der Waals (vdW), $U_{i,\text{vdw}}$, contributions as

$$U_i(z) = U_{i,\text{elec}}(z) + U_{i,\text{vdw}}(z). \tag{4}$$

Procedures to determine $U_{i,\text{elec}}$ and $U_{i,\text{vdw}}$ are described in Subsections II A and II B.

A. Electrostatic potential

To include the effects of water orientation polarization and dielectric permittivity variation on the electrostatic potential, we model water molecules as point-like Langevin dipoles (LDs) as described by Gongadze *et al.*[28] The electrostatic potentials for the ions and water molecules are determined as

$$U_{+/-,\text{elec}}(z) = q_{+/-}\phi(z), \tag{5a}$$

$$U_{\text{w,elec}}(z) = \mu\,\langle\cos\theta(z)\rangle\,\phi'(z), \tag{5b}$$

where q_+ and q_- are the charges on the cation and anion, respectively, ϕ is the mean electrostatic potential, $\phi'(z) = \frac{d\phi(z)}{dz}$, μ is the dipole moment of the water molecule, θ is the angle between the water dipole vector and the z-axis, and $\langle\cos\theta(z)\rangle$

is the average cosine of the dipole orientation. $\langle\cos\theta(z)\rangle$ can be computed as (see Ref. 28)

$$\langle\cos\theta(z)\rangle = -\mathcal{L}\left(\beta\mu\phi'(z)\right), \tag{6}$$

where $\mathcal{L}(x) = \left(\coth x - \frac{1}{x}\right)$ is the Langevin function and $\beta = \frac{1}{k_B T}$.

From the average dipole orientation profile, we can determine the orientation polarization, $P(z)$, and the dielectric permittivity variation, $\varepsilon_r(z)$, as

$$P(z) = \rho_w(z)\mu\langle\cos\theta(z)\rangle \tag{7}$$

and

$$\varepsilon_r(z) = 1 - \frac{P(z)}{\varepsilon_0\phi'(z)}, \tag{8}$$

where ε_0 is the vacuum dielectric constant. In the limit of $\phi'(z) \to 0$, Eq. (8) reduces to the bulk dielectric permittivity,

$$\lim_{\phi'(z)\to 0} \varepsilon_r(z) = \varepsilon_{r,b} = 1 + \frac{\rho_{w,b}\mu^2\beta}{3\varepsilon_0}, \tag{9}$$

where $\varepsilon_{r,b}$ is the bulk dielectric permittivity and $\rho_{w,b}$ is the bulk density of water. We note that the definition of the permittivity given by Eq. (8) (the Clausius-Mosotty formula) is valid for the bulk homogeneous and weakly inhomogeneous systems.[30] For strong inhomogeneous systems, a local average density based phenomenological expression for $\varepsilon_r(z)$ is proposed which smoothens out the strong oscillations in the dielectric permittivity profile predicted by Eq. (8).[30,41] However, MD simulation studies have shown that, near a wall, the dielectric permittivity of water exhibits strong oscillations similar to the density of water.[24,42] Therefore, in this work, we use Eq. (8) which depends on the local density value of water and results in the dielectric permittivity oscillations similar to the oscillations in the density of water (see Sec. V A and Fig. 6).

To compute $\phi(z)$, we use the 1-D Poisson equation with spatially varying dielectric permittivity as

$$\frac{d}{dz}\left(\varepsilon_r(z)\frac{d\phi}{dz}\right) = -\frac{q_+\rho_+(z) + q_-\rho_-(z)}{\varepsilon_0}, \tag{10}$$

with boundary conditions

$$\left.\frac{d\phi}{dz}\right|_{z=0} = -\frac{\sigma_{\text{wall-L}}}{\varepsilon_0}, \tag{11a}$$

$$\left.\frac{d\phi}{dz}\right|_{z=L} = \frac{\sigma_{\text{wall-U}}}{\varepsilon_0}, \tag{11b}$$

$$\phi(z = L/2) = 0. \tag{11c}$$

In Eqs. (10) and (11), $\sigma_{\text{wall-L}}$ and $\sigma_{\text{wall-U}}$ are the surface charge densities of the lower ($z = 0$) and upper ($z = L$) walls, respectively. To obtain a non-trivial solution of the Poisson equation with the constant surface charge boundary conditions (Eqs. (11a) and (11b), we impose a zero potential condition at the mid-point of the channel via Eq. (11c). Therefore, $\phi(z)$ is the relative electrostatic potential with respect to the mid-point of the channel. The condition of $\phi(L/2) = 0$ is generally exact for sufficiently large channels with significant bulk-like region in the center. However, for smaller channels in which EDLs of opposite walls may overlap, Eq. (11c) may not be exact. In such cases, to determine a unique solution of Eq. (10), it is simpler to use constant surface potential boundary conditions instead of constant surface charge boundary conditions.

B. vdW potential

We compute the total vdW potential as a sum of the wall-fluid, $U^{\text{wf}}_{i,\text{vdw}}$ and fluid-fluid, $U^{\text{ff}}_{i,\text{vdw}}$, vdW potentials as

$$U_{i,\text{vdw}}(z) = U^{\text{wf}}_{i,\text{vdw}}(z) + U^{\text{ff}}_{i,\text{vdw}}(z). \tag{12}$$

In the continuum approximation, we represent the wall as a continuous medium with a uniform particle density, ρ_{wall}. Then, the wall-fluid vdW potential is determined as

$$U^{\text{wf}}_{i,\text{vdw}}(\boldsymbol{r}) = \rho_{\text{wall}}\int u^{\text{wf}}_i(r)d\boldsymbol{r}', \tag{13}$$

where $u^{\text{wf}}_i(r)$ is the effective vdW pair potential between the wall atoms and molecule i, $\boldsymbol{r}$ and $\boldsymbol{r}'$ are the position vectors, and $r = |\boldsymbol{r} - \boldsymbol{r}'|$. A procedure to compute $U^{\text{wf}}_{i,\text{vdw}}(\boldsymbol{r})$ for a slit-channel system is described in Ref. 39. Note that in Eq. (13), $\boldsymbol{r} = x\boldsymbol{i} + y\boldsymbol{j} + z\boldsymbol{k}$ is a general position vector. In the case of a 1-D slit channel, the system is periodic in x and y dimensions and therefore, we consider only the z-variations of the properties, i.e., $U^{\text{wf}}_{i,\text{vdw}}(\boldsymbol{r}) = U^{\text{wf}}_{i,\text{vdw}}(x, y, z) = U^{\text{wf}}_{i,\text{vdw}}(z)\ \forall\ x, y$.

The fluid-fluid vdW potentials are more challenging to compute than the wall-fluid potentials. They give rise to the finite size, i.e., excluded volume effects, dispersion attraction, and particle-particle correlations in the fluid. The exact theoretical framework, which accounts for all the fluid-fluid interaction effects, is unknown. In this work, we split the fluid-fluid vdW potential into purely repulsive and dispersion components as

$$U^{\text{ff}}_{i,\text{vdw}}(\boldsymbol{r}) = U^{\text{ff}}_{i,\text{hs}}(\boldsymbol{r}) + \sum_{j=1}^{3}\int_{R^{\text{ff}}_{ij,\text{min}}}^{R^{\text{ff}}_{ij,\text{cut}}} \rho_j(\boldsymbol{r}')u^{\text{ff}}_{ij}(r)d\boldsymbol{r}', \tag{14}$$

where $u^{\text{ff}}_{ij}(r)$ is the effective vdW pair potential between fluid molecules i and j, and $R^{\text{ff}}_{ij,\text{min}}$ and $R^{\text{ff}}_{ij,\text{cut}}$ are the inner and outer cut-offs for the dispersion part of the pair potential, respectively. In Eq. (14), $U^{\text{ff}}_{i,\text{hs}}(\boldsymbol{r})$ is the purely repulsive component of the fluid-fluid interactions, which mainly accounts for the excluded volume effects. We use the hard sphere fluid approximation based on the White-Bear version of fundamental measure theory (FMT) mark II[43] to determine $U^{\text{ff}}_{i,\text{hs}}(r)$ as

$$U^{\text{ff}}_{i,\text{hs}}(\boldsymbol{r}) = k_B T\sum_\alpha \int d\boldsymbol{r}'\frac{\partial\Phi\left(\{n_\alpha\}\right)}{\partial n_\alpha}\frac{\delta n_\alpha(\boldsymbol{r}')}{\delta\rho_i(\boldsymbol{r})}, \tag{15}$$

where Φ is the reduced free energy density and $\{n_\alpha\}$ are the set of weighted densities. The details about Φ and $\{n_\alpha\}$ are given in the Appendix. The second term in Eq. (14) accounts for the fluid-fluid vdW attractive interactions using a mean field approximation.

To compute $U^{\text{wf}}_{i,\text{vdw}}$ and $U^{\text{ff}}_{i,\text{vdw}}$, we need to specify $u^{\text{wf}}_i(r)$ and $u^{\text{ff}}_{ij}(r)$. In Eqs. (13) and (14), $u^{\text{wf}}_i(r)$ and $u^{\text{ff}}_{ij}(r)$ are assumed to be spherically symmetric isotropic pair potentials. Classical atomistic force fields, which are used in MD simulations, provide vdW pair potentials for wall-fluid and fluid-fluid interactions. In the atomistic force fields, vdW interactions of ions are commonly modeled with the pair additive LJ potentials. For monoatomic ions, the ion-ion and ion-wall LJ potentials are

spherically symmetric and hence, they are straightforward to use in Eqs. (13) and (14). However, in MD, the water molecule is generally modeled with multiple sites to represent hydrogen and oxygen atoms and partial charge distribution, e.g., three sites SPC/E model,[44] four sites TIP4P model,[45] and five sites TIP5P model.[46] Due to multiple sites per water molecule, the water-water and ion-water interactions in an atomistic force field are anisotropic, i.e., they depend not only on the separation distance between molecules but also on the relative orientation. Therefore, it is more complex to use fully atomistic force field of water in a continuum framework. Hence, we need a simple yet accurate potential model for water which can incorporate the effects of water polarization and ion-water interactions. As explained in Sec. II A, in EQT, we use a point dipole model for water to include polarization effects of water. However, as per our knowledge, there is no point dipole-based force field for water which can accurately predict the structural and dielectric properties of water. Therefore, we first develop a point dipole-based water force field and single site spherically symmetric ion-water coarse-grained potentials as described in Sec. III.

III. COARSE-GRAINED (CG) POTENTIALS

We follow a systematic coarse-graining approach to develop a point dipole based CG model of water and obtain ion-water CG interactions. Systematic coarse-graining is a bottom-up approach to devise CG models by systematically linking a low resolution CG system to a reference high resolution all atom (AA) system.[47–49] In this work, we first obtain the CG potentials in the particle based CG MD framework and use the same CG interactions in EQT to compute the water-water and ion-water vdW potentials.

A. Point dipole CG water model

To mimic point dipoles in CG MD, we use an extended dipole topology as shown in Fig. 1, in which two opposite charges, $\pm q$, are symmetrically placed at distance $d/2$ from the center of the molecule. Ballenegger and Hansen[50] have shown that for $d/\sigma_{\text{mol}} \leq 0.25$, the extended dipole and point dipole models are similar, where σ_{mol} is the effective diameter of the molecule. For the dipole water model, we fix $d = 0.058$ nm, which is same as the length of the SPC/E water dipole, and it also satisfies $d/\sigma_{\text{mol}} = 0.183 \leq 0.25$ (with $\sigma_{\text{mol}} = \sigma_{\text{SPCE}} = 0.317$ nm). Therefore, the dipole water model has a permanent dipole moment of $\mu = qd$. Total interaction energy between two extended dipoles is a sum of the four electrostatic interactions between the point charges and the vdW interactions,

$$U_{ij,\text{dd}} = u_{\text{dd,cg}}\left(r_{ij}\right) + \sum_{l=1}^{2}\sum_{m=1}^{2} \frac{q_{il}q_{jm}}{4\pi\varepsilon_0 \left|\boldsymbol{r}_{il} - \boldsymbol{r}_{jm}\right|}, \tag{16}$$

where $U_{ij,\text{dd}}$ is the total interaction energy between two dipoles i and j, $u_{\text{dd,cg}}(r_{ij})$ is the coarse-grained vdW pair potential, r_{ij} is the center-to-center distance between i and j dipoles, q_{il} and q_{jm} are the point charges of dipole molecules i and j, respectively, $q_{i1} = q_{j1} = -q$ and $q_{i2} = q_{j2} = +q$, and $\boldsymbol{r}_{il}$ and $\boldsymbol{r}_{jm}$ are the positions of q_{il} and q_{jm}, respectively. Therefore, the vdW interaction between two dipoles depends only on the distance between the centers of the dipoles, and hence, it is spherically symmetric.

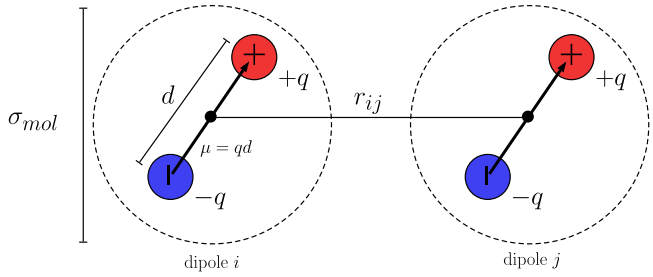

FIG. 1. Topology of the extended dipole water molecule.

For an accurate prediction of EDL properties, we need a dipole model which can accurately capture the structural and dielectric properties of water. We use systematic coarse-graining to determine q and $u_{\text{dd,cg}}(r)$ for the point dipole model such that it reproduces the radial distribution function (RDF) and dielectric permittivity of the bulk water. We use SPC/E as a reference AA model and the RDF of bulk water at 298 K and 1.0 g/cm^3 thermodynamic state as the target RDF and 78.5 as the target permittivity.

There are various structure-based systematic coarse-graining techniques, such as iterative Boltzmann inversion (IBI),[51] inverse Monte Carlo (IMC),[52] and relative entropy minimization,[53,54] which can optimize $u_{\text{dd,cg}}(r)$ to reproduce a target RDF. We use the relative entropy minimization method to optimize $u_{\text{dd,cg}}(r)$. We model $u_{\text{dd,cg}}(r)$ with a cubic B-spline functional form (see Ref. 55 for the details of the B-spline potential). In Ref. 54, it is shown that when CG pair potentials are modeled using finely tabulated functional forms, such as B-splines, the relative entropy minimization based CG potentials reproduce RDFs. Relative entropy based CG water models have been shown to accurately predict the RDF of the bulk water[55,56] and the density profiles of the confined water.[40] However, the relative entropy minimization does not guarantee reproducibility of the dielectric permittivity. We note that the dielectric permittivity mainly depends on the magnitude of the dipole moment, $\mu = qd$. Since, as mentioned above, we fix $d = 0.058$ nm, q is the only free parameter to adjust μ. We use a trial and error approach to optimize q such that the target permittivity is reproduced. In this approach, we first set a test value for $q = q^{\text{t}}$ and perform the relative entropy minimization to obtain the vdW pair potential, $u_{\text{dd,cg}}(r) = u^{\text{t}}_{\text{dd,cg}}(r)$, corresponding to q^{t}. Then we perform a CG MD simulation with q^{t} and $u^{\text{t}}_{\text{dd,cg}}(r)$ and compute the RDF and dielectric permittivity. We perform different sets of relative entropy-based coarse-graining calculations with different point charge values. We note that for each point charge value the relative entropy method is able to determine the pair potential which reproduces the target RDF.

Fig. 2 shows different pair potentials for different point charge values and comparison of RDFs. We observe that all of them are able to reproduce the target RDF. Dielectric permittivity values obtained for the different combinations of the point charge and pair potential are given in Table I. We choose the CG potential obtained with $q = 0.73$ e, which reproduces both the target RDF and dielectric permittivity.

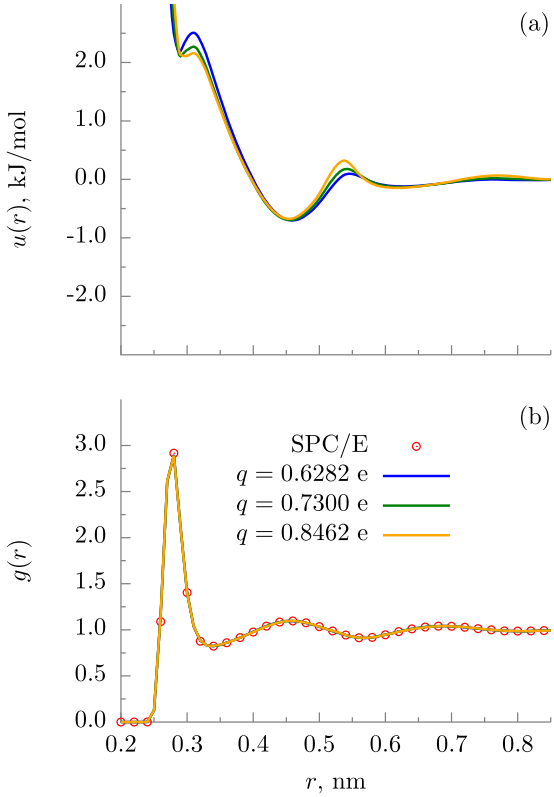

FIG. 2. (a) Dipole-dipole CG potentials obtained by the relative entropy minimization for different point charge values. (b) Comparison of COM RDFs from SPC/E based AA MD and point dipole based CG MD.

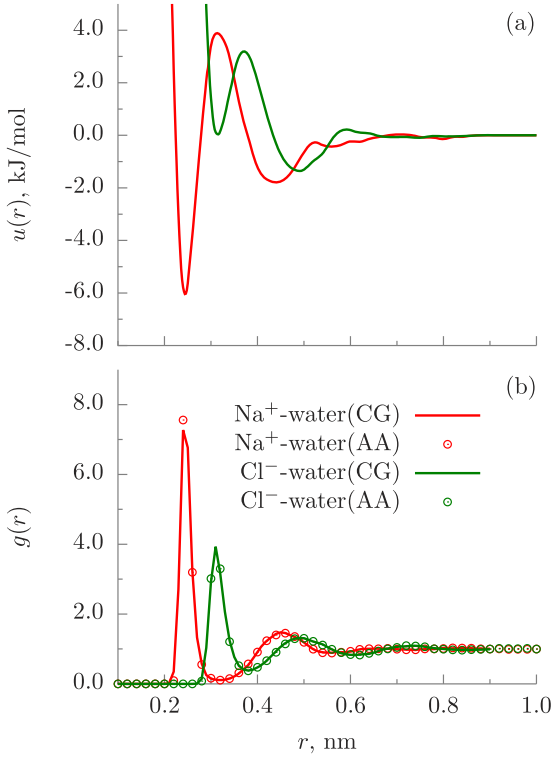

FIG. 3. (a) Ion-water CG potentials obtained by relative entropy minimization. (b) Comparison of ion-water RDFs from AA MD and CG MD.

B. Ion-water CG potentials

An ion-water interaction has two parts: (i) the long-range ion-water electrostatic interaction and (ii) the short-range ion-water vdW interaction. The ion-water electrostatic interaction causes screening of the ion-ion electrostatic interactions. The effects of the ion-water electrostatic interactions can be accounted via the dielectric permittivity of water, which scales down (i.e., screens) the ion-ion electrostatic interactions. Therefore, here, we only determine the ion-water short-range vdW interactions by the systematic coarse-graining approach.

For systematic coarse-graining of the ion-water vdW interactions, we use a single Na^+–Cl^- pair dissolved in a bulk water system. In the reference atomistic simulations, water is modeled with SPC/E force field; ion-ion and ion-water interactions are modeled with the force field of Joung and Cheatham[57] (see Sec. IV B). To determine the ion-water CG interactions, we represent water as a single bead and for water-water interactions, we use the relative entropy based CG interactions obtained in Ref. 55. The ion-ion vdW interactions are the same as the LJ interactions in the atomistic force-field. The charges on the ions are also kept the same as in the atomistic force field. The ion-ion electrostatics are computed by the particle mesh Ewald (PME)[58] method with the relative permittivity of 78.5. The ion-water CG potentials are modeled with B-splines and optimized by the relative entropy minimization.

Fig. 3 shows the Na^+-water and Cl^--water CG potentials and the comparison of the ion-water RDFs from the AA MD and CG MD simulations. We observe that the ion-water CG potentials accurately predict the ion-water RDFs. Though the ion-water CG potentials are obtained from the single ion pair system, i.e., dilute ion concentration, we find that the ion-water CG potentials are transferable up to 1M ion concentration, i.e., they can reproduce ion-water RDFs of the bulk NaCl system up to 1M concentration.

In this work, the relative entropy-based coarse-graining for the point dipole CG water and ion-water CG interactions is performed using the versatile object-oriented toolkit for coarse-graining applications (VOTCA).[55,59] We follow the procedure as described in Ref. 55 for the relative entropy minimization. The reference AA MD and CG MD simulations are performed in GROMACS.[60] The long-range electrostatic interactions are computed with the PME. A cutoff of 0.9 nm is used for the vdW pair potential and the short-range component of the electrostatic interactions.

TABLE I. Dielectric permittivities of point dipole water for different point charge values.

q (e)	μ (D)	ε_r
0.8476	2.35	292.78
0.7300	2.034	77.01
0.6282	1.75	49.75

IV. SIMULATION DETAILS

To demonstrate EQT for EDL, we simulate the NaCl aqueous electrolyte confined inside slit-like capacitor channels. The electrolyte fluid is confined between two parallel, uniformly, and oppositely charged graphene walls separated by 3.804 nm

TABLE II. Summary of the systems simulated.

System no.	Lower/upper wall charge density (C/m^2)	NaCl concentration (M)	Molecules in MD simulations water/Na^+/Cl^-
I	−0.12/0.12	0.25	1624/14/14
II	−0.15/0.15	0.50	1637/22/22
III	−0.15/0.15	0.75	1633/28/28
IV	−0.18/0.18	1.00	1640/37/37

(=$12\sigma_{OW}$, where σ_{ow}(=0.317 nm) is the length scale of the LJ interactions between water oxygen atoms). $12\sigma_{ow}$ is a large enough width to avoid overlap of two opposite EDLs and allow sufficiently wide bulk-like region at the center of the channel. The confined electrolyte is assumed to be in thermodynamic equilibrium with a reference bulk electrolyte system. We consider a range of 0.25M–1M bulk ion concentrations in water at 1.0 g/cm^3 density and 298 K temperature, and surface charge densities of 0.12–0.18 C/m^2. Table II summarizes four different systems considered in this work. To check the accuracy of EQT, we compare the EQT results with MD simulations.

A. EQT simulations

In EQT, we solve Eqs. (3)–(14) self-consistently to determine density and potential profiles of ions and water. The reference densities and potentials required in Eq. (3) are determined from the reference bulk system. The reference bulk potentials, $U_{i,\mathrm{ref}}$, are computed by substituting the bulk densities in Eq. (14). To compute the attractive part of the vdW potential from Eq. (14), we use the CG pair potentials, i.e.,

$$u^{\mathrm{ff}}_{ij}(r) = u^{\mathrm{ff}}_{ij,\mathrm{cg}}(r), \tag{17}$$

where $u^{\mathrm{ff}}_{ij,\mathrm{cg}}$ is the CG interaction between the molecules i and j. As explained in Sec. II B, for the ion-ion pairs, $u^{\mathrm{ff}}_{ij,\mathrm{cg}}$ are the same LJ potentials as in the reference MD simulations (see Sec. IV B), and for the water-water and ion-water pairs, we use the CG pair potentials obtained in Sec. III. For all the pair potentials, we set $R^{\mathrm{ff}}_{ij,\mathrm{cut}} = 0.9$ nm. There are different approaches to set $R^{\mathrm{ff}}_{ij,\mathrm{min}}$ for the LJ type pair potentials.[61] Here, we set $R^{\mathrm{ff}}_{ij,\mathrm{min}} = \sigma^{\mathrm{ff}}_{ij}$ for the ion-ion LJ pair potentials, where $\sigma^{\mathrm{ff}}_{ij}$ is the usual LJ parameter. For the water-water and ion-water CG potentials, we set $R^{\mathrm{ff}}_{ij,\mathrm{min}}$ to be the location of the first minima of the corresponding CG pair potential. Therefore, $R^{\mathrm{ff}}_{\mathrm{ww,min}} = 0.28$ nm, $R^{\mathrm{ff}}_{\mathrm{+w,min}} = 0.244$ nm, and $R^{\mathrm{ff}}_{\mathrm{-w,min}} = 0.314$ nm. To compute the wall-fluid potential energies from Eq. (13), we use $\rho_{\mathrm{wall}} = 38.18$ atoms/nm^3 for the graphene walls. For the wall-water potential energy, we use the same LJ pair potential as that of C–O pair in the reference MD simulations. For the wall-ion potentials, as explained in Sec. V B, we modify the reference MD C-ion LJ pair potentials to account for the errors in the Langevin dipole model near the walls. To determine the mean electrostatic potential, $\phi(z)$, we solve Eqs. (10) and (11) with $q_+ = +1.0$ e and $q_- = -1.0$ e, and $\mu = 2.88$ D. For the capacitor channel, the walls are equally and oppositely charged such that $\sigma_{\text{wall-L}} = -\sigma_{\mathrm{wall}}$ and $\sigma_{\text{wall-U}} = \sigma_{\mathrm{wall}}$, where σ_{wall} is the given surface charge density. To determine the hard-sphere energy component from FMT (Eq. (15)), we use $d_{\mathrm{hs,w}} = 0.28$ nm, $d_{\mathrm{hs,+}} = 0.14$ nm, and $d_{\mathrm{hs,-}} = 0.23$ nm. The values for μ and $d_{\mathrm{hs},i}$ are set such that the density profiles from EQT compare well with the reference MD simulations. The summary of the interaction parameters used in EQT simulations is given in Table III.

Once all the parameters are set, we use the Picard iteration technique to self-consistently solve Eqs. (3)–(14). We note that the convergence of the Picard iterations depends on the initial guesses for the fluid density profiles. We use uniform bulk fluid densities as an initial guess. However, for high surface charge densities, the Picard iterations may diverge depending on the initial guess. Similar convergence issues for high ion concentrations and surface charge densities have been observed by others.[30,32] To solve the convergence issue, we implement a surface charge stepping procedure as following. We start with a zero surface charge boundary condition and uniform bulk densities as an initial guess and obtain the converged fluid densities, $\rho^0_i(z)$, corresponding to the zero surface charge. Next, we increment the surface charge by a discrete value $\Delta\sigma_{\mathrm{wall}}$ and use $\rho^0_i(z)$ as an initial guess to again obtain the converged densities, $\rho^{\Delta\sigma_{\mathrm{wall}}}_i(z)$. We repeat this procedure of increasing the surface charge by $\Delta\sigma_{\mathrm{wall}}$ and using $\rho^{(n-1)\Delta\sigma_{\mathrm{wall}}}_i(z)$ as an initial guess to obtain the density profiles for the surface charge of $n\Delta\sigma_{\mathrm{wall}}$ until we reach the target surface charge value, σ_{wall}.

TABLE III. Interaction parameters in EQT simulations.

	q (e)	μ (D)	d_{hs} (nm)
Water	0.0	2.88	0.28
Na^+	+1.0	0.0	0.14
Cl^-	−1.0	0.0	0.23
	$u^{\mathrm{ff}}_{\mathrm{cg}}(r)$	$R^{\mathrm{ff}}_{\mathrm{min}}$ (nm)	
Water–Water	$u_{\mathrm{dd,cg}}(r)$[a]	0.28	
Na^+–Na^+	$u_{\mathrm{Na–Na,md}}(r)$[b]	0.215 95	
Cl^-–Cl^-	$u_{\mathrm{Cl–Cl,md}}(r)$[b]	0.483 04	
Na^+–Cl^-	$u_{\mathrm{Na–Cl,md}}(r)$[b]	0.349 495	
Na^+–Water	$u_{\mathrm{Na–Water,cg}}(r)$[c]	0.244	
Cl^-–Water	$u_{\mathrm{Cl–Water,cg}}(r)$[c]	0.314	
C–Water	$u_{\mathrm{C–O,md}}(r)$[b]	0.0	
C–Na^+	LJ (σ = 0.4596 nm, ϵ = 0.2328 kJ/mol)	0.0	
C–Cl^-	LJ (σ = 0.3814 nm, ϵ = 0.1781 kJ/mol)	0.0	

[a]Same as the dipole-dipole CG potential obtained in Sec. III A.
[b]Same as the LJ potentials in MD (Table IV).
[c]Same as the ion-water CG potentials obtained in Sec. III B.

We note that the EQT simulations are orders of magnitude faster than the MD simulations. For example, on a single Intel Core i7-3520M 4M Cache 3.60 GHz processor, an EQT simulation of system III requires around 4 min, whereas a 10 ns long MD simulation of the same system requires around 60 h.

B. MD simulations

The reference MD simulations are performed in the *NVT* (canonical) ensemble by GROMACS. Two graphene walls are placed along the *xy* plane, and the lateral dimensions of the walls are $3.834 \times 3.689\,27\ \text{nm}^2$. The wall atoms are kept fixed. A uniform partial charge is assigned to the wall atoms. The value of the partial charge on the wall atoms is determined from a given surface charge density. For example, −0.02 e and +0.02 e charges are assigned to the lower ($z = 0$) and upper ($z = L$) wall atoms, respectively, to achieve the surface charge density of $0.12\ \text{C/m}^2$. Periodic boundary conditions are used in the x, y, and z directions. Water is modeled using the SPC/E force field, and ions are modeled using the force field of Joung and Cheatham.[57] The LJ interaction parameters of various fluid particles are given in Table IV. The LJ parameters between two dissimilar particles are determined by the Lorentz-Berthlot (LB) combination rule. We note that Wu and Aluru[62] have developed a more accurate graphitic carbon-water force field. This carbon-water force field depends on the water orientation and hence, it is anisotropic. As explained in Sec. II B, for simplicity, we use isotropic vdW pair potentials in EQT, and therefore, in MD also, we model C-water interactions by the LJ type isotropic pair potential parameters given in Table IV. A spherical cutoff of 0.9 nm is used for the LJ interactions, and electrostatic interactions are computed by PME.[58] The simulation box is padded with a vacuum layer of $50\sigma_{ow}$ in the z dimension along with a correction for the slab geometry to exclude the interactions between the periodic images in z. Temperature is maintained using the Nosé-Hoover thermostat[63] with 0.5 ps time constant. Equations of motion are integrated with the leap-frog algorithm with a time step of 1 fs. For a given bulk ion concentration and surface charge density, the number of ions and water molecules is determined by a trial and error approach such that the bulk fluid densities are achieved in the center of the channel. The number of molecules determined for different systems are given in Table II. For each ion concentration and surface charge density, equilibrium properties are obtained by averaging the values from 5 different MD simulations of 10 ns each with different initial conditions.

TABLE IV. LJ interaction parameters in MD simulations.

	σ (nm)[a]	ϵ (kJ/mol)[a]
H	0.0	0.0
O	0.317	0.650 3
Na^+	0.215 95	1.475 45
Cl^-	0.483 04	0.053 49
C	0.339	0.233 4

[a]Parameters for the two dissimilar particles are determined by the Lorentz-Berthlot (LB) combination rule.

V. RESULTS AND DISCUSSION

A. Analysis of LD approach

First, we analyze the ability of the LD model to predict electrostatic potential variations in EDL. For this analysis, we provide the ion and water center of mass (COM) density profiles from the MD simulations of system II as an input to the LD Eqs. (6)–(11) and solve the equations self-consistently. To study the dependence of LD results on the dipole moment, we vary μ from 1.2 to 4.8 D. For comparison, we also compute $\phi(z)$ with a uniform dielectric permittivity of $\epsilon_r = 78.5$. We compare $\phi(z)$ from the LD and uniform permittivity approaches with MD. To compute $\phi(z)$ from MD, we solve Eq. (10) with $\epsilon_r = 1$ and the charge densities of ions and partial charges of water molecules, i.e., $\sum_i q_i \rho_i(z) = q_{Na^+}\rho_{Na^+}(z) + q_{Cl^-}\rho_{Cl^-}(z) + q_H\rho_H(z) + q_O\rho_O(z)$. Fig. 4 shows the total charge density and densities of Na^+, Cl^-, O, H, and water COM from MD.

Fig. 5 shows the comparison of the electrostatic potentials from MD, LD, and uniform permittivity approaches. We observe that $\phi(z)$ from MD shows pronounced oscillations near the channel walls and it varies linearly in the central region of the channel. In the lower half of the channel, i.e., closer to the negatively charged wall, $\phi(z)$ is mostly negative except at 0.2 nm away from the lower wall, where there is a positive peak in $\phi(z)$. The positive peak in the electrostatic potential near the negatively charged wall can be attributed to the net positive charge density due to the accumulation of positively charged hydrogen atoms at 0.2 nm away from the lower wall

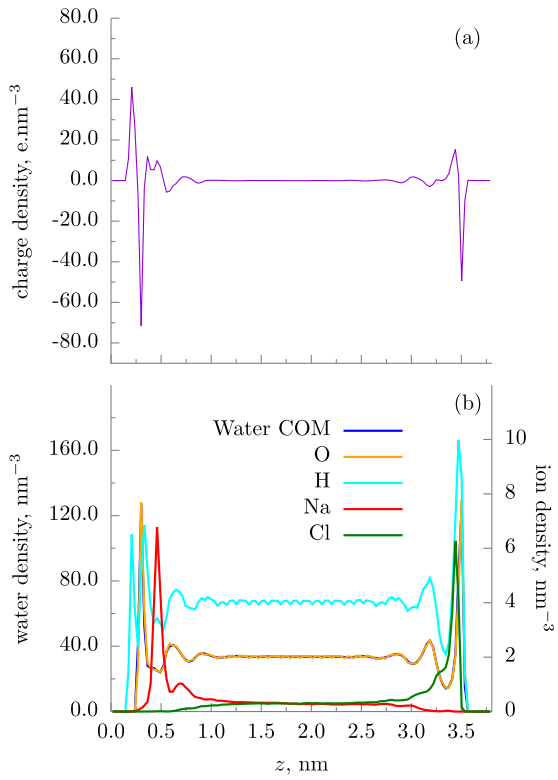

FIG. 4. Charge and species density profiles from the MD simulations of system II: (a) Total charge density, i.e., ions plus water partial charges. (b) O, H, and water COM densities on the left y-axis and Na^+ and Cl^- ion densities on the right y-axis.

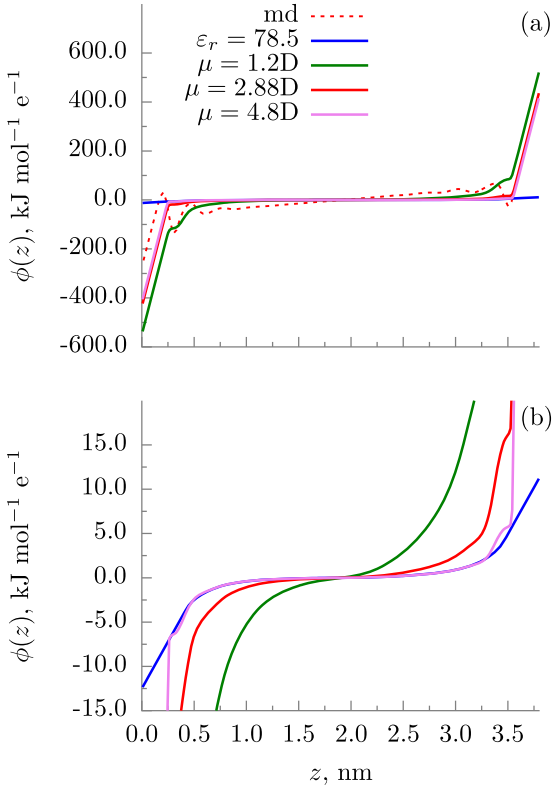

FIG. 5. Electrostatic potentials for system II from MD, LD with different dipole moment values, and uniform permittivity approximation with $\varepsilon_r = 78.5$. (a) Full range plots for comparison with MD. (b) Zoomed in plot for comparing LD and uniform permittivity approaches.

(see Fig. 4). Similarly, in the upper half of the channel, $\phi(z)$ is mostly positive except at 0.3 nm away from the upper wall, where there is a negative valley due to the net negative charge density from the accumulation of negatively charged Cl^- and oxygen atoms.

The electrostatic potential profiles from the LD approach show weaker oscillations compared to MD. Moreover, the strength of the electrostatic potential from the LD model decreases as the dipole moment value is increased. This behavior can be understood by examining the dielectric permittivity profiles from the LD model for different μ values as shown in Fig. 6. We observe that, for all μ values, the variations in ε_r are similar to the variations in the water COM density

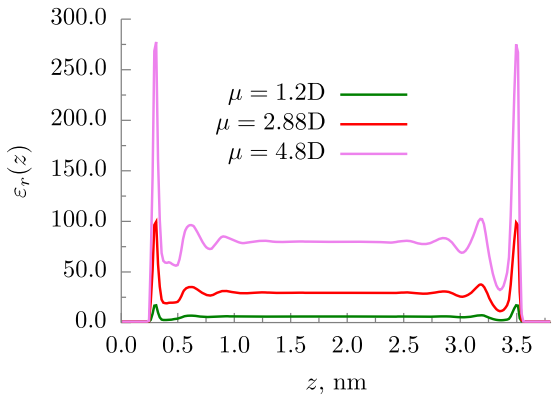

FIG. 6. Dielectric permittivity profiles of system II from LD with different dipole moment values.

profile. However, a larger dipole moment value results in a higher permittivity profile which results in a stronger screening of the surface electric field and hence, a smaller potential profile. The errors in the LD model are due to the simplifications adopted in Eqs. (6)–(10). The LD model is a mean-field approach, and hence, it ignores dipole-dipole direct interactions and dipole-dipole correlations.[28] In addition, the LD model neglects higher electric moments of the water molecule, such as a quadrupole moment, which also contribute to the dielectric permittivity variation of confined water.[24,25]

Though the LD model fails to capture the oscillations in $\phi(z)$, the surface potentials at the walls (i.e., $\phi(0)$ and $\phi(L)$) predicted by LD are comparable to MD. We observe that, for all μ values considered, the error in the surface potential at the negatively charged wall is higher compared to the error at the positively charged wall. This is mainly due to the failure of the LD framework to capture the positive peak in the electrostatic potential near the negatively charged wall. Despite these errors, the LD framework performs better than the uniform dielectric approach. From Fig. 5, we observe that $\phi(z)$ from the uniform dielectric permittivity approach does not exhibit any oscillations and it increases monotonically from the lower to the upper wall. Moreover, there is an order of magnitude error in the surface potentials predicted by the uniform permittivity approach. Therefore, the LD approach is an improvement over the uniform permittivity approach.

B. EQT results

We use the EQT framework to obtain ion and water density profiles for the four systems summarized in Table II. The numerical details of the EQT simulations are given in Sec. IV A. As explained in Sec. IV A, for the ion-ion interactions, we use the same LJ potentials that are used in the reference MD simulations. For the water-water and ion-water pair interactions, we use the systematically developed CG potentials discussed in Sec. III. For the wall-water interactions, we use the same C–O LJ potential used in the reference MD simulations. For the wall-ion interactions, we use LJ pair potentials similar to those in the reference MD. However, we modify the wall-ion LJ interaction parameters to account for the errors in the electrostatic potential near the walls due to the approximations in the LD model as described in Sec. V A. To optimize the wall-ion LJ potentials, we use a potential of mean force (PMF) matching based technique.[40] For the PMF-matching, we use system IV as a reference system. The optimized wall-ion LJ parameters are as follows: $\sigma_+^{wf} = 0.4596$ nm, $\epsilon_+^{wf} = 0.2328$ kJ/mol, $\sigma_-^{wf} = 0.3814$ nm, and $\epsilon_-^{wf} = 0.1781$ kJ/mol. For the water point dipole, we use $\mu = 2.88$ D because it predicts the surface electrostatic potentials comparable to MD (see Sec. V A). The summary of the interaction parameters used in EQT simulations is given in Table III.

Figs. 7 and 8 show the comparison of the density profiles from EQT and MD for water and ions, respectively. For comparison purposes, we also include the density profiles from 3CM cDFT simulations. In the 3CM cDFT simulations, water molecules are modeled as neutral LJ type particles, and ions are modeled as charged particles with LJ interactions. The LJ

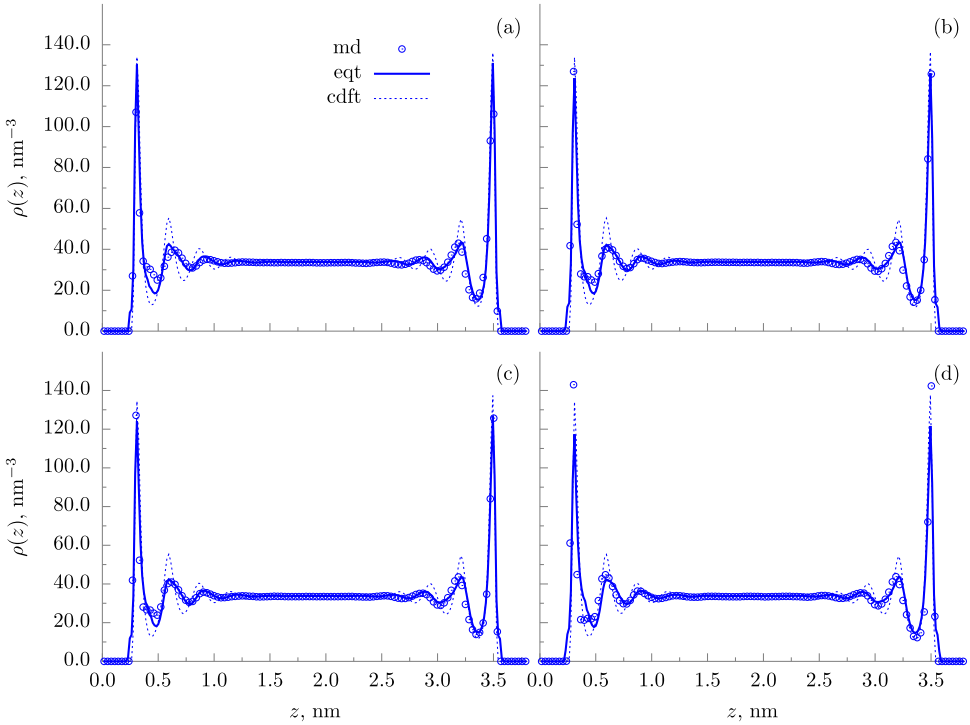

FIG. 7. Comparison of water density profiles from EQT, 3CM cDFT, and MD for four different systems: (a) system I, (b) system II, (c) system III, and (d) system IV.

interaction parameters are the same as in MD, and the electrostatic interactions are computed by the Poisson's equation with a uniform dielectric permittivity of 78.5. The hard sphere component of the free energy is modeled with FMT with the same hard sphere diameters as in EQT.

Fig. 7 shows that the water density profiles from EQT compare well with the reference MD simulations. The 3CM cDFT predicts higher oscillations in the water density profiles compared to MD. The errors in the 3CM cDFT water density profiles are due to the simple LJ based model of water, which ignores the water-water electrostatic interactions. Fig. 8 shows that the ion density profiles from EQT compare well with the reference MD simulations. The distribution of Na^+ and Cl^- ions near the charged surfaces, such as the location of the first peak and layering, is different due to the differences in their sizes and hydration properties.[21,64,65] Such ion specific information is built into the EQT framework via different hard sphere diameters and ion-water CG potentials, which accounts for the ion hydration. The ion density profiles from 3CM cDFT are qualitatively and quantitatively different than the MD simulations. The errors in the 3CM cDFT mainly arise from the inability of the simple LJ based ion-water potentials

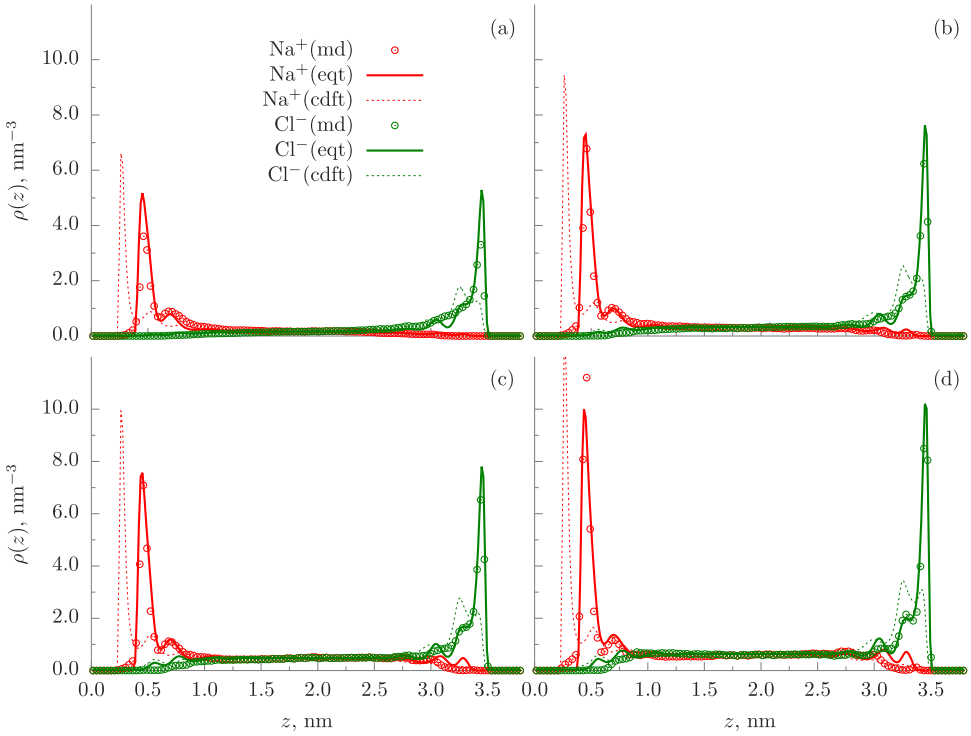

FIG. 8. Comparison of Na^+ and Cl^- ion density profiles from EQT, 3CM cDFT, and MD for four different systems: (a) system I, (b) system II, (c) system III, and (d) system IV.

and uniform dielectric permittivity assumption to capture ion hydration and water polarization effects.

There are, however, some quantitative discrepancies between the EQT and MD density profiles. These discrepancies are due to the simplifications made in this work. In addition to the mean-field approximations in the LD approach, as described in Sec. V A, we ignore fluid-fluid correlations while determining the vdW potentials from Eq. (14). Also, for the water-water and ion-water interactions, we use the CG potentials determined from the bulk systems. Since, the interfacial arrangement of the water molecules and ions is different from the bulk, the bulk-based CG potentials are not exact near the surface. There are approaches in EQT to address these limitations. The fluid-fluid correlation effects can be accounted via the correlation correction potential approach as described in Refs. 36 and 37. To account for the errors arising from the bulk-based CG potentials near the interface, wall-fluid interactions can be modified as suggested in Refs. 39 and 40. We note that, in this work, we already optimize the wall-ion LJ interactions to account for the errors near the interface. The accuracy of these wall-ion CG potentials can further be improved by using a more flexible B-spline functional form. Similarly, the errors in the water density profiles can be corrected by using a more complex functional form, such as LJ plus 2 Gaussians or B-splines, to model the wall-water vdW potential.[39,40]

VI. CONCLUSIONS

In this work, we developed a realistic explicit water based theoretical framework for studying EDLs. This framework is based on the EQT and point dipole based coarse-grained water model. In EQT, water polarization and dielectric permittivity variations are modeled using the Langevin dipole approach. Finite size effects of water and ions are approximated by the White-Bear mark II (WBII) version of FMT. To accurately capture hydration interactions, we systematically developed water-water and ion-water coarse-grained potentials by relative entropy minimization. We demonstrated EQT by simulating the NaCl aqueous electrolyte confined inside slit-like capacitor channels for various ion concentrations and surface charge densities. EQT predictions of the water and ion density profiles agree well with the reference MD simulations. Further improvements can be made to the EQT framework presented in this work by incorporating dipole-dipole direct interactions and dipole-dipole and fluid-fluid correlations.

ACKNOWLEDGMENTS

This work was supported by AFOSR (Grant No. FA9550-12-1-0464) and by NSF (Grant Nos. 1264282, 1420882, 1506619, and 1545907). The authors acknowledge the use of the Taub cluster provided by the Computational Science and Engineering Program at the University of Illinois.

APPENDIX: FUNDAMENTAL MEASURE THEORY

Rosenfeld's fundamental measure theory (FMT) provides a functional to determine the excess (over the ideal gas) free energy of hard-sphere mixtures, $F_{\text{hs}}\left[\{\rho_i\}\right]$, as[43,66]

$$\beta F_{\text{hs}}\left[\{\rho_i\}\right] = \int d\boldsymbol{r}' \Phi\left(\{n_\alpha\left(\boldsymbol{r}'\right)\}\right), \tag{A1}$$

where $\beta = \frac{1}{k_B T}$, Φ is the reduced free energy density, and $\{n_\alpha\}$ are the set of weighted densities. The weighted densities for the ν-component mixture are defined as

$$n_\alpha\left(\boldsymbol{r}\right) = \sum_i^\nu \int d\boldsymbol{r}' \rho_i\left(\boldsymbol{r}'\right) \omega_\alpha^i\left(\boldsymbol{r}-\boldsymbol{r}'\right), \tag{A2}$$

where ω_α^i are the weight functions given by

$$\begin{aligned}
\omega_3^i\left(\boldsymbol{r}\right) &= \Theta\left(R_{i,\text{hs}} - r\right), \\
\omega_2^i\left(\boldsymbol{r}\right) &= \delta\left(R_{i,\text{hs}} - r\right), \\
\boldsymbol{\omega}_2^i\left(\boldsymbol{r}\right) &= \frac{\boldsymbol{r}}{r}\delta\left(R_{i,\text{hs}} - r\right), \\
\omega_1^i\left(\boldsymbol{r}\right) &= \frac{\omega_2^i\left(\boldsymbol{r}\right)}{4\pi R_{i,\text{hs}}}, \\
\omega_0^i\left(\boldsymbol{r}\right) &= \frac{\omega_2^i\left(\boldsymbol{r}\right)}{4\pi R_{i,\text{hs}}^2}, \\
\boldsymbol{\omega}_1^i\left(\boldsymbol{r}\right) &= \frac{\boldsymbol{\omega}_2^i\left(\boldsymbol{r}\right)}{4\pi R_{i,\text{hs}}}.
\end{aligned} \tag{A3}$$

In Eq. (A3), $R_{i,\text{hs}} = \frac{d_{i,\text{hs}}}{2}$ is the hard-sphere radius of the molecule i, $d_{i,\text{hs}}$ is the hard-sphere diameter of the molecule i, $\Theta(r)$ is the Heaviside step function, $\delta(r)$ is the Dirac-delta distribution, and $r = |\boldsymbol{r}|$. The integrations over ω_α^i (Eq. (A2)) give the *fundamental measures* of a fluid i, such as the volume ($\alpha = 3$), the surface area ($\alpha = 2$), the mean radius of curvature ($\alpha = 1$), and the Euler characteristics ($\alpha = 0$).

Various functions for the reduced free energy density, $\Phi\left(\{n_\alpha\left(\boldsymbol{r}'\right)\}\right)$, are derived from the different thermodynamic conditions.[43] For example, the original Rosenfeld functional based on the scaled-particle theory equation, the White-Bear (WB) functional based on the Mansoori-Carnahan-Starling-Leland (MCSL) equation of state, and the White-Bear mark II (WBII) functional, which is similar to the WB functional but is constructed to reproduce the Carnahan-Starling-Boublík equation of state for a one-component bulk fluid. In this work, we use the WBII version of FMT. In WBII, the reduced free energy density is given by

$$\begin{aligned}
\Phi = &-n_0 \ln\left(1-n_3\right) + \left(n_1 n_2 - \boldsymbol{n}_1 \cdot \boldsymbol{n}_2\right) \frac{1 + \frac{1}{3}\phi_2\left(n_3\right)}{1-n_3} \\
&+ \left(n_2^3 - 3 n_2 \boldsymbol{n}_2 \cdot \boldsymbol{n}_2\right) \frac{1 - \frac{1}{3}\phi_3\left(n_3\right)}{24\pi(1-n_3)^2},
\end{aligned} \tag{A4}$$

where

$$\phi_2\left(n_3\right) = \frac{1}{n_3}\left(2n_3 - n_3^2 + 2\left(1-n_3\right)\ln\left(1-n_3\right)\right) \tag{A5}$$

and

$$\phi_3\left(n_3\right) = \frac{1}{n_3^2}\left(2n_3 - 3n_3^2 + 2n_3^3 + 2(1-n_3)^2 \ln\left(1-n_3\right)\right). \tag{A6}$$

From Eqs. (A1) and (A2), we determine $U_{i,\text{hs}}^{\text{ff}}$, required in Eq. (14), as

$$U^{\mathrm{ff}}_{i,\mathrm{hs}}(\boldsymbol{r}) = \frac{\delta F_{\mathrm{hs}}\left[\{\rho_i\}\right]}{\delta \rho_i(\boldsymbol{r})} = k_{\mathrm{B}}T \sum_{\alpha} \int d\boldsymbol{r}' \frac{\partial \Phi\left(\{n_\alpha\}\right)}{\partial n_\alpha} \frac{\delta n_\alpha(\boldsymbol{r}')}{\delta \rho_i(\boldsymbol{r})}. \tag{A7}$$

For a 1-D slit channel, the weighted densities expression, Eq. (A2), simplifies to[43]

$$n_\alpha(\boldsymbol{r}) = n_\alpha(z) = \sum_i \int dz' \rho_i(z') \omega^i_\alpha(z - z'), \tag{A8}$$

where the one dimensional weight functions are

$$\begin{aligned}
\omega^i_3(z) &= \pi\left(R_i^2 - z^2\right)\Theta\left(R_i - |z|\right), \\
\omega^i_2(z) &= 2\pi R_i \Theta\left(R_i - |z|\right), \\
\boldsymbol{\omega}^i_2(z) &= 2\pi z \boldsymbol{e}_z \Theta\left(R_i - |z|\right), \\
\omega^i_1(z) &= \frac{\omega^i_2(z)}{4\pi R_i}, \\
\omega^i_0(z) &= \frac{\omega^i_2(z)}{4\pi R_i^2}, \\
\boldsymbol{\omega}^i_1(z) &= \frac{\boldsymbol{\omega}^i_2(z)}{4\pi R_i},
\end{aligned} \tag{A9}$$

where $\boldsymbol{e}_z$ is the unit vector in the z-direction. Similarly, the expression for $U^{\mathrm{ff}}_{i,\mathrm{hs}}$, Eq. (A7), simplifies to

$$U^{\mathrm{ff}}_{i,\mathrm{hs}}(z) = \frac{\delta F_{\mathrm{hs}}\left[\{\rho_i\}\right]}{\delta \rho_i(z)} = k_{\mathrm{B}}T \sum_{\alpha} \int dz' \frac{\partial \Phi\left(\{n_\alpha\}\right)}{\partial n_\alpha} \frac{\delta n_\alpha(z')}{\delta \rho_i(z)}. \tag{A10}$$

To evaluate the integrations in Eqs. (A8) and (A10), we use the numerical scheme given by Knepley *et al.*[67]

[1] J. Lyklema, *Fundamentals of Interface and Colloid Science* (Academic Press, 1995), Vol. 2, pp. 3-1–3-232.
[2] B. E. Conway, *Electrochemical Supercapacitors Scientific Fundamentals and Technological Applications* (Springer, USA, 1999).
[3] P. Simon and Y. Gogotsi, Nat. Mater. **7**, 845 (2008).
[4] M. A. Shannon, P. W. Bohn, M. Elimelech, J. G. Georgiadis, B. J. Marias, and A. M. Mayes, Nature **452**, 301 (2008).
[5] M. Heiranian, A. B. Farimani, and N. R. Aluru, Nat. Commun. **6**, 8616 (2015).
[6] B. Hille, *Ion Channels of Excitable Membranes* (Sinauer, 2001).
[7] R. Qiao and N. R. Aluru, J. Chem. Phys. **118**, 4692 (2003).
[8] D. Kim and E. Darve, Phys. Rev. E **73**, 051203 (2006).
[9] H.-J. Butt, K. Graf, and M. Kappl, *Physics and Chemistry of Interfaces* (Wiley-VCH Verlag GmbH & Co. KGaA, 2003), pp. 42–56.
[10] I. Borukhov, D. Andelman, and H. Orland, Phys. Rev. Lett. **79**, 435 (1997).
[11] R. Kjellander, T. Åkesson, B. Jönsson, and S. Marčelja, J. Chem. Phys. **97**, 1424 (1992).
[12] R. Evans and T. J. Sluckin, Mol. Phys. **40**, 413 (1980).
[13] J. Wu, AIChE J. **52**, 1169 (2006).
[14] J. W. Lee, R. H. Nilson, J. A. Templeton, S. K. Griffiths, A. Kung, and B. M. Wong, J. Chem. Theory Comput. **8**, 2012 (2012).
[15] A. L. Frischknecht, D. O. Halligan, and M. L. Parks, J. Chem. Phys. **141**, 054708 (2014).
[16] J. W. Lee, A. Mani, and J. A. Templeton, Langmuir **31**, 7496 (2015).
[17] K. M. Salerno, A. L. Frischknecht, and M. J. Stevens, J. Phys. Chem. B **120**, 5927 (2016).
[18] J. Jiang, D. Cao, D. Henderson, and J. Wu, J. Chem. Phys. **140**, 044714 (2014).
[19] Z. Tang, L. Mier-y-Teran, H. T. Davis, L. E. Scriven, and H. S. White, Mol. Phys. **71**, 369 (1990).
[20] P. Kékicheff, S. Marčelja, T. J. Senden, and V. E. Shubin, J. Chem. Phys. **99**, 6098 (1993).
[21] R. Qiao and N. R. Aluru, Phys. Rev. Lett. **92**, 198301 (2004).
[22] J. Marti, G. Nagy, M. C. Gordillo, and E. Gurdia, J. Chem. Phys. **124**, 094703 (2006).
[23] M. F. Chaplin, *in Adsorption and Phase Behaviour in Nanochannels and Nanotubes,* edited by P. L. J. Dunne and D. G. Manos (Springer, Netherlands, 2010), pp. 241–255.
[24] D. J. Bonthuis, S. Gekle, and R. R. Netz, Phys. Rev. Lett. **107**, 166102 (2011).
[25] D. J. Bonthuis and R. R. Netz, J. Phys. Chem. B **117**, 11397 (2013).
[26] S. Lamperski and A. Zydor, Electrochim. Acta **52**, 2429 (2007).
[27] T. Goel, C. N. Patra, S. K. Ghosh, and T. Mukherjee, J. Chem. Phys. **129**, 154906 (2008).
[28] E. Gongadze, A. Velikonja, Š. Perutkova, P. Kramar, A. Maček-Lebar, V. Kralj-Iglič, and A. Iglič, Electrochim. Acta **126**, 42 (2014).
[29] E. Gongadze and A. Iglič, Electrochim. Acta **178**, 541 (2015).
[30] V. Warshavsky and M. Marucho, Phys. Rev. E **93**, 042607 (2016).
[31] L. Blum and D. Henderson, J. Chem. Phys. **74**, 1902 (1981).
[32] D. Henderson, D.-e. Jiang, Z. Jin, and J. Wu, J. Phys. Chem. B **116**, 11356 (2012).
[33] D. Henderson and D. Boda, Phys. Chem. Chem. Phys. **11**, 3822 (2009).
[34] A. V. Raghunathan, J. H. Park, and N. R. Aluru, J. Chem. Phys. **127**, 174701 (2007).
[35] T. Sanghi and N. R. Aluru, J. Chem. Phys. **132**, 044703 (2010).
[36] S. Y. Mashayak, M. H. Motevaselian, and N. R. Aluru, J. Chem. Phys. **142**, 244116 (2015).
[37] M. H. Motevaselian, S. Y. Mashayak, and N. R. Aluru, J. Chem. Phys. **143**, 124106 (2015).
[38] T. Sanghi and N. R. Aluru, J. Chem. Phys. **136**, 024102 (2012).
[39] S. Y. Mashayak and N. R. Aluru, J. Chem. Theory Comput. **8**, 1828 (2012).
[40] S. Y. Mashayak and N. R. Aluru, J. Chem. Phys. **137**, 214707 (2012).
[41] A. Oleksy and J.-P. Hansen, Mol. Phys. **107**, 2609 (2009).
[42] V. Ballenegger and J.-P. Hansen, J. Chem. Phys. **122**, 114711 (2005).
[43] R. Roth, J. Phys.: Condens. Matter **22**, 063102 (2010).
[44] H. J. C. Berendsen, J. R. Grigera, and T. P. Straatsma, J. Phys. Chem. **91**, 6269 (1987).
[45] W. L. Jorgensen and J. D. Madura, Mol. Phys. **56**, 1381 (1985).
[46] M. W. Mahoney and W. L. Jorgensen, J. Chem. Phys. **112**, 8910 (2000).
[47] C. Peter and K. Kremer, Soft Matter **5**, 4357 (2009).
[48] G. A. Voth, *Coarse-Graining of Condensed Phase and Biomolecular Systems* (CRC Press, 2008).
[49] W. G. Noid, J. Chem. Phys. **139**, 090901 (2013).
[50] V. Ballenegger and J.-P. Hansen, Mol. Phys. **102**, 599 (2004).
[51] D. Reith, M. Pütz, and F. Müller-Plathe, J. Comput. Chem. **24**, 1624 (2003).
[52] A. P. Lyubartsev and A. Laaksonen, Phys. Rev. E **52**, 3730 (1995).
[53] M. S. Shell, J. Chem. Phys. **129**, 144108 (2008).
[54] A. Chaimovich and M. S. Shell, J. Chem. Phys. **134**, 094112 (2011).
[55] S. Y. Mashayak, M. N. Jochum, K. Koschke, N. R. Aluru, V. Rühle, and C. Junghans, PLoS One **10**, e0131754 (2015).
[56] A. Chaimovich and M. S. Shell, Phys. Chem. Chem. Phys. **11**, 1901 (2009).
[57] I. S. Joung and T. E. Cheatham, J. Phys. Chem. B **112**, 9020 (2008).
[58] T. Darden, D. York, and L. Pedersen, J. Chem. Phys. **98**, 10089 (1993).
[59] V. Rühle, C. Junghans, A. Lukyanov, K. Kremer, and D. Andrienko, J. Chem. Theory Comput. **5**, 3211 (2009).
[60] S. Pronk, S. Páll, R. Schulz, P. Larsson, P. Bjelkmar, R. Apostolov, M. R. Shirts, J. C. Smith, P. M. Kasson, D. v. d. Spoel *et al.*, Bioinformatics **29**, 845 (2013).
[61] J. D. Weeks, D. Chandler, and H. C. Andersen, J. Chem. Phys. **54**, 5237 (1971).
[62] Y. Wu and N. R. Aluru, J. Phys. Chem. B **117**, 8802 (2013).
[63] S. Nosé, J. Chem. Phys. **81**, 511 (1984).
[64] R. Qiao and N. Aluru, Colloids Surf., A **267**, 103 (2005).
[65] G. Feng, R. Qiao, G. Hu, and N. R. Aluru, *Computational Bioengineering* (CRC Press, 2015), pp. 327–353.
[66] Y. Rosenfeld, Phys. Rev. Lett. **63**, 980 (1989).
[67] M. G. Knepley, D. A. Karpeev, S. Davidovits, R. S. Eisenberg, and D. Gillespie, J. Chem. Phys. **132**, 124101 (2010).